

Structural phase transitions in SrTiO₃ nanoparticles

Han Zhang, Sizhan Liu, Megan E. Scofield, Stanislaus S. Wong, Xinguo Hong, Vitali B. Prakapenka, Eran Greenberg, and Trevor A. Tyson

Citation: *Appl. Phys. Lett.* **111**, 052904 (2017); doi: 10.1063/1.4997332

View online: <http://dx.doi.org/10.1063/1.4997332>

View Table of Contents: <http://aip.scitation.org/toc/apl/111/5>

Published by the [American Institute of Physics](#)

Articles you may be interested in

[Periodic arrays of flux-closure domains in ferroelectric thin films with oxide electrodes](#)
Applied Physics Letters **111**, 052901 (2017); 10.1063/1.4996232

[Nonlinear electrostrictive lattice response of EuTiO₃](#)
Applied Physics Letters **111**, 052902 (2017); 10.1063/1.4996494



CiSE magazine is an innovative blend.

The advertisement features a stylized circuit diagram with three main components labeled: 'COMPUTING' (represented by a blue line), 'ENGINEERING' (represented by a green line), and 'SCIENCE' (represented by a purple line). The lines are interconnected, with the 'ENGINEERING' line forming a series of loops. To the right, there is a small image of the magazine cover, which has the title 'Computing - SCIENCE - ENGINEERING' and the subtitle 'EXPLORING OUR SOLAR SYSTEM'. The cover art depicts a rocket launching from Earth towards a red planet in space.

Structural phase transitions in SrTiO₃ nanoparticles HPSTAR 491-2017

Han Zhang,¹ Sizhan Liu,¹ Megan E. Scofield,² Stanislaus S. Wong,^{2,3} Xinguo Hong,^{4,5}
 Vitali B. Prakapenka,⁶ Eran Greenberg,⁶ and Trevor A. Tyson^{1,a)}

¹Department of Physics, New Jersey Institute of Technology, Newark, New Jersey 07102, USA

²Department of Chemistry, State University of New York at Stony Brook, Stony Brook, New York 11794-3400, USA

³Condensed Matter Physics and Materials Science Division, Brookhaven National Laboratory, Upton, New York 11973, USA

⁴Mineral Physics Institute, Stony Brook University, Stony Brook, New York 11794, USA

⁵Center for High Pressure Science and Technology Advanced Research, Beijing 100094, People's Republic of China

⁶Center for Advanced Radiation Sources, University of Chicago, Chicago, Illinois 60637, USA

(Received 29 April 2017; accepted 23 July 2017; published online 4 August 2017)

Pressure dependent structural measurements on monodispersed nanoscale SrTiO₃ samples with average diameters of 10 to ~80 nm were conducted to enhance the understanding of the structural phase diagram of nanoscale SrTiO₃. A robust pressure independent polar structure was found in the 10 nm sample for pressures up to 13 GPa, while a size dependent cubic to tetragonal transition occurs (at $P=P_c$) for larger particle sizes. The results suggest that the growth of ~10 nm STO particles on substrates with significant lattice mismatch may maintain a polar state for a large range of strain values, possibly enabling device use. *Published by AIP Publishing.* [<http://dx.doi.org/10.1063/1.4997332>]

Perovskites form a particularly interesting class of materials because even slight modifications of the crystal structure can lead to dramatic changes in physical properties, such as superconductivity, ferroelectricity, and ferromagnetism. Strontium titanate, SrTiO₃ (STO), is considered to be a model perovskite and plays an important role in the understanding of soft-mode-driven phase transitions, which have been extensively studied for more than five decades.

SrTiO₃ is known as an incipient ferroelectric material, with its pure form remaining paraelectric down to ~0 K. Small perturbations of the structure, such as but not limited to isotope substitution,¹ chemical doping,² the application of electric fields,³ and/or stress,⁴ can result in the onset of a ferroelectric state at finite temperatures. For example, isotopic substitution with ¹⁸O yields a system having a ferroelectric transition temperature with $T_c \sim 23$ K. A large enhancement of T_c was first reported by Haeni *et al.*⁵ When applying tensile strain in STO epitaxial films, a ferroelectric transition can be observed above room temperature. Additionally, anisotropically strained STO thin films on a GdScO₃ substrate were reported to have a ferroelectric transition as high as 400 K.⁶ It has also been reported that the phase transition behavior and domain structure in anisotropically strained STO thin films differ significantly compared with isotropically strained films. According to a study conducted by Jang *et al.*, the role of strain is to stabilize longer range correlations of pre-existing nanopolar regions (PNRs),⁷ related to unintentional Sr deficiency.

The bulk STO system is cubic under ambient conditions. However, the oxygen atoms located in the octahedral sites can easily rotate around the central titanium atom, thereby giving rise to possible distortions of the cubic crystal.⁸ An antiferrodistortive (AFD) transition to a non-polar tetragonal phase occurs at ~105 K at ambient pressure in bulk samples.

This temperature-induced phase transition has been intensively examined,⁹ both experimentally and theoretically, with a soft phonon mode model proposed to describe the observed transition. The AFD transition can also be affected by applying pressure (see [supplementary material](#)).

Studies of simple nanoscale perovskites have been conducted, with the aim of utilizing them in device applications for high-density storage ([supplementary material](#)). In our recent work conducted on various sizes of STO nanoparticles, a polar state over a wide temperature range (20–300 K, possibly with ferroelectric properties) was found in free-standing 10 nm nanoparticles.¹⁰ More recently, a scaled reduction of STO thin films was found to have produced ferroelectricity.¹¹ We note that while a large body of research has previously been conducted on STO films and on the BaTiO₃ system, very limited studies on the atomic structure, ferroelectricity, and the polar state of STO nanoparticles have been carried out. Nanoscale STO can potentially possess unique properties that are not exhibited by either bulk or film systems.

To assess this system in reduced dimensions, a systematic study of STO nanoparticles possessing various particle sizes is needed. In this work, therefore, the phase diagram of STO nanoparticles will be constructed by analyzing and studying samples, incorporating a broad range of average particle diameters, under varying pressure conditions. Particles averaging 20 nm to ~83 nm in diameter are found to exhibit size-dependent structural phase transitions, which occur at lower pressures as the particle size is reduced. Conversely, 10 nm particles exhibit a robust pressure-independent polar structure for pressures of up to 13 GPa. Experimental details can be found in the [supplementary material](#).

Figure S2 in the [supplementary material](#) shows representative intensity vs. 2θ XRD patterns (see also Fig. S1 in the [supplementary material](#)). The transformation to 2θ -space revealed that the peaks from the pattern of the 83 nm sample illustrated in Fig. S2(a) ([supplementary material](#)) are sharper

^{a)}Author to whom correspondence should be addressed: tyson@njit.edu

than those from the 20 nm sample, presented in Fig. S2(b) (supplementary material), mainly due to the difference in the particle size.¹² The signal from the Ne pressure medium was marked as * in Fig. S2(b) (supplementary material). With this exception, no new peaks appear over the whole measured pressure range. Rietveld refinements were performed on the collected XRD data to obtain the structural parameters of the STO particles. The profiles of the refinement (data fit) under ambient pressure for the 83 nm and 20 nm samples are shown in Figs. 1(a) and 1(b). The 2θ values of Fig. 1(b) have been re-calculated for easy comparison. A high χ^2 value of the refinement in Fig. 1(b) was obtained mainly due to the background subtracted before refinement (see Ref. 13). Typical χ^2 values for 10 nm and 83 nm STO are ~ 0.2 over the pressure range measured.

To better understand the correlation between pressure and particle size, 3rd order equation of state (EOS) fits using the Birch-Murnaghan (BM) equation $P(V) = \frac{3B_0}{2} \left[\left(\frac{V_0}{V} \right)^{\frac{2}{3}} - \left(\frac{V_0}{V} \right)^{\frac{5}{3}} \right] \left\{ 1 + \frac{3}{4} (B'_0 - 4) \left[\left(\frac{V_0}{V} \right)^{\frac{2}{3}} - 1 \right] \right\}$ were performed with the results presented in Fig. 2, where B_0 is the bulk modulus and B'_0 is the derivative with respect to pressure. The error in pressure determination can be found in the supplementary material. The order of the BM-EOS was determined by examination of the Normalized pressure F vs. Eulerian strain f plot (not shown) with the program EosfitGUI.¹⁴ The error of the lattice was extracted directly from Rietveld refinement as the uncertainty in fit parameters. We note that the standard uncertainty from Rietveld refinement is typically smaller than the real error.¹⁵

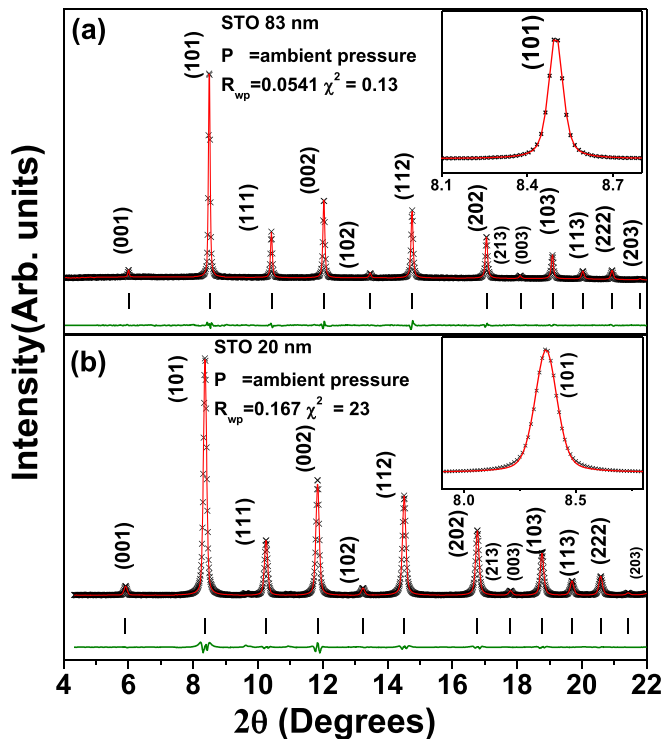


FIG. 1. Rietveld refinement results at ambient pressure for (a) 83 nm and (b) 20 nm STO. The observed (crosses), calculated (solid line), and difference (bottom line) patterns are shown. The vertical bars show the peak positions for the refined model. The 2θ values of (b) have been re-calculated for easy comparison. The insets show an expanded region for the (101) peak.

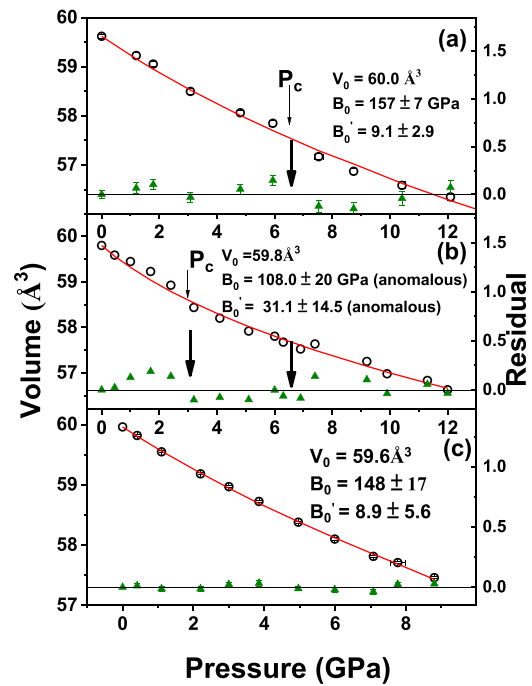


FIG. 2. (a) The third order Birch-Murnaghan equation of state fit (solid lines) of experimental results (circles) and the residual (green triangles) between 0 and 12 GPa for 83 nm STO, with a deviation that can be observed above ~ 6 GPa. (b) Single model fit for the 20 nm sample over the entire pressure range. (c) Single model fit for the 10 nm sample. The deviations from the low-pressure phase are more evident in the peak width variations (Fig. 3).

Figure 2(a) highlights the fitting curve using the 3rd order BM-EOS between 0 and 12 GPa, showing that data points were clearly off the curve at a certain pressure,¹⁶ indicated as P_c . The residual (difference between the fit and the data) shown as the lower plot in each panel reveals a sudden change near 6–7 GPa. The bulk modulus B_0 and its pressure derivative B'_0 obtained from the fit are $B_0 = 157 \pm 7$ GPa and $B'_0 = 9.1 \pm 2.9$, respectively. B'_0 is slightly out of the normal range, with typical values corresponding to B'_0 between 2 and 8.¹⁷ The value of B_0 can be compared with the corresponding value of other well-studied perovskites, which are listed in Table S1 in the supplementary material. It can be observed that although the 83 nm sample possesses a structural transition near 6 GPa, which is similar to the bulk value, the bulk modulus is significantly smaller than that of the bulk sample (~ 220 GPa). (The deviation at 6 GPa is more evident in the diffraction peak widths, Fig. 3.) This result can be caused by the size effects associated with the nanoscale particles. The expansion of the STO lattice with reduced size suggests a lattice softening with size reduction, consistent with the B_0 reduction. The expansion is due to the reduction of the hybridization of the oxygen p and titanium d bands (see previous work in the supplementary material of Ref. 10). This behavior is also observed in Ref. 18, in which the decrease in the electrostatic force caused by the valence reduction of Ce ions and an increase in the ionicity of Ti ions were argued to be the reason for the observed lattice expansions in CeO_{2-x} and BaTiO_3 nanoparticles, respectively. A similar analysis was not conducted with the 40 nm sample, due to the lower 2θ range with that data set, as mentioned in

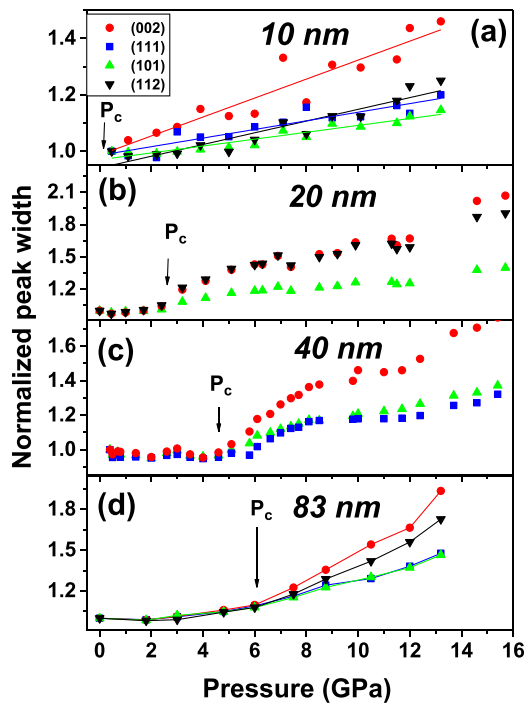


FIG. 3. Specified peak widths vs. pressure for the STO system extracted from the diffraction patterns for particle sizes (a) 10 nm, (b) 20 nm, (c) 40 nm, and (d) 83 nm, respectively. There is a clear shift of the transition pressure (P_c) towards the lower pressure region with decreasing particle size.

the experimental details. By examining the data associated with the 20 nm sample, as shown in Fig. 2(b), a deviation (transition) is observed but is shifted towards a lower pressure value of ~ 2.5 GPa. A 3rd order BM-EOS over the entire pressure range yields a B'_0 value of >30 , which is not correct and strongly suggests a structural phase transition during the compression. Meanwhile, refinement of the data above 2.5 GPa yields $B_0 \sim 9.1 \pm 3.6$ (not shown in the plot). Looking at the residual curve, we also note that there is a possible additional transition near ~ 7 GPa.

Figure 2(c) presents the 3rd order BM-EOS fit for the 10 nm STO sample. The experimental data can be well described by a single equation in the whole pressure range (no significant deviations in the residual curves), which is quite different from the 83 nm sample. The good agreement of the data with the fitting curve suggests no structural transition in this pressure range. The pressure derivative B'_0 extracted from the refinement is 8.9 ± 5.6 , which is at the upper limit of results for standard oxides. This enhancement is typical of anisotropic compression.¹⁹ This behavior is in good agreement with our previously reported work¹⁰ that demonstrated that the 10 nm STO sample is polar over a wide temperature range. The peak widths reveal the structural changes with pressure more clearly.

To more clearly view the pressure-dependent structural change, we further investigated the XRD pattern by examining the change in peak widths as a function of pressure (looking for splitting/broadening caused by structural transitions to low-symmetry phases).²⁰ In this work, we first fitted some chosen peaks with a Lorentzian profile and then retrieved the corresponding peak width vs. pressure curve. The results are displayed in Fig. 3. Figure 3(a) includes the peak width vs.

pressure data for the (112), (002), (111), and (101) peaks, which can be attributed to the 10 nm STO sample. The 10 nm sample yields no obvious trends which can be observed through the entire pressure range of all of these four peaks. The (112) and (002) peaks exhibit an almost linear response between ambient pressure and 13 GPa, suggesting that the sample structure is stable in this pressure range. However, as we increased the STO particle size, there are clear deviations in the graphs [Figs. 3(b)–3(d)]. For example, for the 20 nm sample, all four peaks maintain almost the same width ratio up to ~ 2.5 GPa, but a sudden increase is observed near ~ 2.5 GPa in the (112) and (002) peaks, which is likely related to the structural transition from the cubic to the tetragonal phase.²⁰ This finding serves as strong evidence that the 20 nm STO has given rise to a pressure-induced structural phase transition at ~ 2.5 GPa. As the particle size is increased, the transition pressure is seen to shift towards the higher pressure region. In Fig. 3(c), the transition pressure is found to be ~ 4.5 GPa for the 40 nm sample, and in Fig. 3(d), the pressure is noted to be ~ 6.0 GPa for the 83 nm sample.

The above results here indicate that 10 nm STO also has a stable tetragonal polar state up to 10 GPa, while the other STO nanoparticles have a cubic to tetragonal transition at a pressure which decreases with decreasing particle size. This work focuses on the structural transition (cubic to tetragonal distortions), but the nature of this transition needs to be determined by future experiments including pressure dependent Raman, x-ray absorption, and neutron scattering measurements. These combined measurements will enable the determination of the phonon modes as a function of pressure to make connections with the polar state (ferroelectric or AFD²¹). Our previous study using Raman spectroscopy, x-ray absorption spectroscopy, and high-resolution x-ray diffraction¹⁰ indicate that the nanoparticles are stoichiometric. For the materials studied in this work, pair distribution function measurements and x-ray absorption measurements (see Figs. S5 and S6 in the supplementary material) further indicate no observable chemical defects or any additional structural phases.

We investigated the transition pressure as a function of different particle sizes, based on the bond-order-length-strength theory developed by Chen *et al.*,²² correlating pressure-induced changes with size-induced changes in the transition temperature. The relationship between the transition pressure P_{cj} and the particle size K_j is found to be related by the following expression: $P_{cj} \sim P_{cb} \left(C1 - \frac{C2}{K_j} \right)$, where P_{cb} is the transition pressure of the bulk sample and $C1$ and $C2$ are constants determined by the nature of the chemical bonding inside the sample.

The theory suggests a linear correlation between the transition pressure and the inverse of the particle size. Examination of Fig. 4(b) reveals that this prediction holds for this system. These combined results are found in Figs. 3 and 4 and give corroborative evidence for our previous conclusion that the 20 nm, 40 nm, and 83 nm STO samples exhibit a pressure-induced phase transition whose onset appears to decrease with decreasing particle size, whereas the 10 nm STO is stable (in a polar phase) between ambient

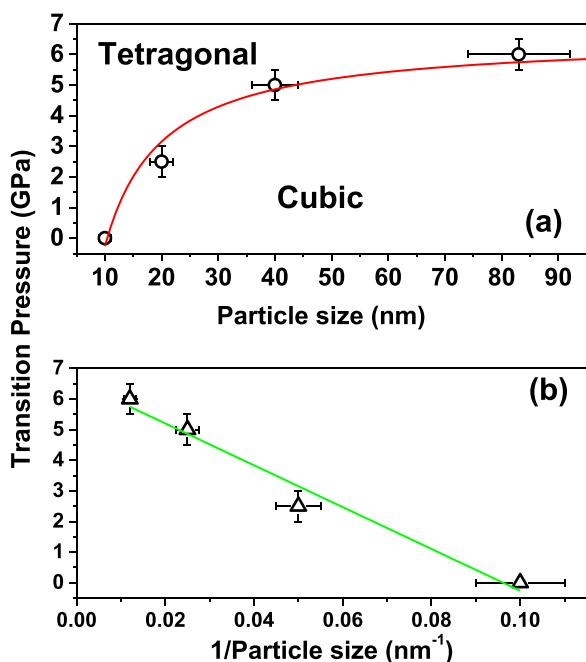


FIG. 4. Phase diagram of SrTiO₃ nanoparticles, with transition pressure vs. (a) particle size and (b) inverse of the particle size. The solid lines are fits based on the simple model results in Ref. 22 (see text).

pressure and 13 GPa. The structural phase diagram under pressure is presented as Fig. 4(a). We note that other oxide systems exhibit even more complex phase changes with size and pressure such as TiO₂.²³ However, the stabilization of tetragonal and possibly polar states in STO nanoparticles is the primary feature of this work. Detailed modeling of the nanoparticulate systems by utilizing density functional methods may assist in determining the microscopic level mechanism for the phase change as a function of particle size and pressure and will be the topic of future work.

This result provides insight into the possible application of STO nanoparticles of various sizes in data storage devices. We note that in the BaTiO₃ system, isotropic pressure suppresses the polar state in bulk samples as pressure increases up to 10 GPa, leading to the cubic state for higher pressures.²⁴ In general, anisotropic pressure (strain) enhances the polar phase in ATiO₃ systems, as mentioned above. We note that polar nano-scale STO particles can be synthesized by simple wet chemical methods. One can grow or deposit the nanoparticles (of diameter ~ 10 nm) onto substrates²⁵ with significant lattice mismatch without appreciably altering the polar state.

The application of an electric field to orient the particles followed by annealing may produce a high-density nanoscale array of nano-ferroelectric materials. By controllably depositing the particles onto a densely patterned surface, high capacity storage may be enabled.

In summary, we have conducted pressure-dependent structural measurements (up to ~ 20 GPa) on monodispersed nanoscale samples with average diameters of 10 nm, 20 nm, 40 nm, and 83 nm, respectively. The transition pressure was found to decrease with decreasing particle size, and a robust pressure-independent structure of the 10 nm sample was observed. The results suggest that growth of STO

nanoparticles (with near 10 nm diameter) onto substrates which do not match the underlying STO lattice will not alter the polar state of the system for a large range of strain values, thereby enabling more widespread device use.

This work was supported by the U.S. Department of Energy (DOE) Grant No. DE-FG02-07ER46402. Research support for M.E.S. and S.S.W. was provided by the U.S. Department of Energy, Basic Energy Sciences, Materials Sciences, and Engineering Division. Synchrotron powder x-ray diffraction experiments were performed at Brookhaven National Laboratory's National Synchrotron Light Source (NSLS) and Advanced Photon Source (APS). The use of the NSLS was supported by the U.S. Department of Energy, Office of Science, Office of Basic Energy Sciences, under Contract No. DE-AC02-98CH10886. This research used resources at GeoSoilEnviroCARS (The University of Chicago, Sector 13), Advanced Photon Source (APS), Argonne National Laboratory. GeoSoilEnviroCARS is supported by the National Science Foundation – Earth Sciences (EAR – 1634415) and Department of Energy-GeoSciences (DE-FG02-94ER14466). The Advanced Photon Source is operated for the DOE Office of Science by Argonne National Laboratory under Contract No. DE-AC02-06CH11357. Pair Distribution Function (PDF) measurements were performed by M. W. Terban from the Billinge group of Columbia University at the XPD1 beamline at National Synchrotron Light Source 2 (NSLS2) at Brookhaven National Laboratory, a U.S. Department of Energy (DOE) Office of Science User Facility operated for the DOE Office of Science by Brookhaven National Laboratory under Contract No. DE-SC0012704.

See [supplementary material](#) for additional introduction, synthesis of SrTiO₃ nanoparticles, XRD 2-D detector image, cell parameters vs. pressure in the tetragonal cell (and a-c splitting), table of bulk modulus, PDF results, derivative of Ti K-edge spectra, and Ti-O XAFS peak data.

¹M. Itoh, R. Wang, Y. Inaguma, T. Yamaguchi, Y. J. Shan, and T. Nakamura, *Phys. Rev. Lett.* **82**, 3540 (1999).

²T. Mitsui and W. B. Westphal, *Phys. Rev.* **124**, 1354 (1961).

³P. A. Fleury and J. M. Worlock, *Phys. Rev.* **174**, 613 (1968).

⁴A. F. Devonshire, *Adv. Phys.* **3**, 85 (1954).

⁵J. H. Haeni, P. Irvin, W. Chang, R. Uecker, P. Reiche, Y. L. Li *et al.*, *Nature* **430**, 758 (2004).

⁶A. Vasudevarao, S. Denev, M. D. Bieganski, Y. Li, L. Q. Chen, S. Mckinstry, D. G. Schlom, and V. Gopalan, *Appl. Phys. Lett.* **92**, 192902 (2008).

⁷H. W. Jang, A. Kumar, S. Denev, M. D. Bieganski, P. Maksymovych, C. W. Bark *et al.*, *Phys. Rev. Lett.* **104**, 197601 (2010).

⁸Y. P. Cai, D. Z. Han, and R. Y. Ning, *Chin. J. Chem. Phys.* **23**, 237 (2010).

⁹R. A. Cowley, *Phys. Rev. Lett.* **9**, 159 (1962); W. Taylor and A. F. Murray, *Solid State Commun.* **31**, 937 (1979); D. A. Bruce and W. G. Stirling, *J. Phys. C* **16**, 841 (1983).

¹⁰T. A. Tyson, T. Yu, M. Croft, M. E. Scofield, D. Bobb-Semple, J. Tao, C. Jaye, D. Fischer, and S. S. Wong, *Appl. Phys. Lett.* **105**, 091901 (2014).

¹¹D. Lee, H. Lu, Y. Gu, S.-Y. Choi, S.-D. Li, S. Ryu, T. R. Paudel, K. Song, E. Mikheev, S. Lee, S. Stemmer, D. A. Tenne, S. H. Oh, E. Y. Tsymlal, X. Wu, L.-Q. Chen, A. Gruverman, and C. B. Eom, *Science* **349**, 1314 (2015).

¹²V. K. Pecharsky and P. Y. Zavalij, *Fundamentals of Powder Diffraction and Structural Characterization of Materials* (Springer, 2009).

¹³B. H. Toby, *Powder Diffr.* **21**, 67 (2006).

- ¹⁴J. Gonzalez-Platas, M. Alvaro, F. Nestola, and R. Angel, *J. Appl. Crystallogr.* **49**, 1377 (2016).
- ¹⁵J. F. Berar and P. Lelann, *J. Appl. Cryst.* **24**, 1 (1991).
- ¹⁶Y. Sharma, S. Sahoo, A. K. Mishra, P. Misra, S. P. Pavunny, A. Dwivedi, S. M. Sharma, and R. S. Katiyar, *J. Appl. Phys.* **117**, 094101 (2015).
- ¹⁷V. G. Tyuterev and N. Vast, *Comput. Mater. Sci.* **38**, 350 (2006).
- ¹⁸S. Tsunekawa, K. Ishikawa, Z. Q. Li, Y. Kawazoe, and A. Kasuya, *Phys. Rev. Lett.* **85**, 3440 (2000).
- ¹⁹I. Loa, P. Adler, A. Grzechnik, K. Syassen, U. Schwarz, M. Hanfland, G. K. Rozenberg, P. Gorodetsky, and M. P. Pasternak, *Phys. Rev. Lett.* **87**, 125501 (2001).
- ²⁰P. Parisiades, E. Liarokapis, J. Köhler, A. Bussmann-Holder, and M. Mezouar, *Phys. Rev. B* **92**, 064102 (2015).
- ²¹A. K. Tagantsev, *Phys. Rev. B* **64**, 224107 (2001).
- ²²Z. Chen, C. Q. Sun, Y. Zhou, and G. Ouyang, *J. Phys. Chem. C* **112**, 2423 (2008).
- ²³A. San-Miguel, *Chem. Soc. Rev.* **35**, 876 (2006).
- ²⁴J. P. Itié, B. Couzinet, A. Polian, A. M. Flank, and P. Lagarde, *Europhys. Lett.* **74**, 706 (2006).
- ²⁵K. Tanaka, K. Suzuki, D. Fu, K. Nishizawa, T. Miki, and K. Kato, *Jpn. J. Appl. Phys.* **43**, 6525 (2004); K. I. Mimura and K. Kato, *ibid.* **52**, 09KC06 (2013).